Design of PI sliding mode control for Zeta DC–DC converter in PV system

Rini Nur HASANAH[1]*, Lunde ARDHENTA[1], Tri NURWATI[1], Onny SETYAWATI[1],
Dian Retno SAWITRI[2], Hadi SUYONO[1] and Taufik TAUFIK[3]

[1] Electrical Engineering Department, Universitas Brawijaya, Indonesia
[2] Electrical Engineering Department, Universitas Dian Nuswantoro, Indonesia
[3] Electrical Engineering Department, Cal Poly State University, USA

Abstract. Solar energy has become one of the most potential alternative energies in the world. To convert solar energy into electricity, a photovoltaic (PV) system can be utilized. However, the fluctuation of sunlight intensity throughout the day greatly affects the generated energy in the PV system. A battery may be beneficial to store the generated energy for later use. A DC–DC converter is commonly exploited to produce a constant output voltage during the battery charging process. A Zeta converter is a DC–DC converter which can be used to produce output values above or below the input voltage without changing the polarity. To deal with the inherent non-linearity and time-varying properties of the converter, in this paper the sliding mode control (SMC) is first analyzed and exploited before being integrated with a proportional-integral (PI) control to regulate the output voltage of the PV system. Disturbances are given in the form of changes in input voltage, reference voltage, and load. Voltage deviation and recovery time to reach a steady-state condition of the output voltage after disturbances are investigated and compared to the results using a proportional-integral-differential (PID) controller. The results show that the proposed control design performs faster than the compared PID control method.

Key words: photovoltaic; Zeta converter; sliding mode control; PI sliding surface.

1. INTRODUCTION

The concern for energy saving and environmental protection has resulted in a considerably impressive development of renewable energy. It is also driven by the consideration of creating sustainable development to achieve a sustainable future. Solar energy is one form of renewable energy source, which is very important to human beings. Its potential is abundant in many regions of the world, especially around the equatorial region [1].

Conversion from solar energy into electrical energy can be realized using a photovoltaic (PV) system [2–4]. The rotation of the earth, as well as the evolution of sun movement, make the intensity of solar radiation also vary throughout the day and the year. The resulted sunlight intensity fluctuation greatly affects the output voltage of a PV system.

It is generally desired that the voltage generated by the PV system can be regulated to fulfill the load requirement. One of the possible PV loads considered in this paper is a battery. During the charging process of the battery, a constant voltage is considered. To achieve the constant voltage condition of the input to the battery, DC–DC converters are common to be utilized [5,6].

Some requirements dictate the need of using converters with the capability to operate in both decreasing and increasing modes with respect to their input value. Some widely known converters include Buck–Boost, Cuk, Sepic, and Zeta [7–12]. Buck-Boost and Cuk converters can be used to produce an output voltage which is negatively proportional to the input voltage. To get the same polarity as the input voltage, the problem can be solved by adding an isolated transformer, but with the increasing size and cost.

Sepic and Zeta converters are preferable if it is desired to get an output voltage with the same polarity as the input [11–15]. Zeta converter has been shown to outperform Sepic converter in terms of losses and power factor [16]. Zeta converter also provides low output ripples which facilitate the output regulation task. The involved uniform output current also enables the smaller capacitor requirement to enhance the load performance.

The output voltage of the Zeta converter varies following the variation of the incoming sunlight radiation. Therefore, a controller is needed to provide a constant voltage during the battery charging process. The control objectives can be assigned to maintain the stability of the regulated output voltage and to improve the control performance by providing a desired transient response in a form of minimized overshoot.

Some methods have been reported to deal with nonlinear control problems [17–22]. Sliding mode control (SMC) is one of the most popular control techniques in nonlinear control systems [17–19]. It changes the system dynamics by applying discontinuous control signals, thereby forcing the system to slide along cross-sections of the system normal behavior [19–22]. The complexity of the feedback design can also be reduced due to the possibility to decompose the system motion into independent partial components of lower dimensions [17].

*e-mail: rini.hasanah@ub.ac.id

Bull. Pol. Acad. Sci. Tech. Sci., vol. 70, no. 3, p. e140952, 2022

1

The SMC is commonly used for high-order systems that are continuous. In [11], the use of SMC includes robustness as well as uncertainty issues in its design consideration. It gives additional advantages of being compared to the other feedback control techniques. It also offers another advantage in dealing with parameter variations and disturbances, avoiding having to use exact mathematical models.

Since the beginning, there has been much research carried out on SMC utilization in power converters [23, 24]. It is suitable to be implemented on power converters as it produces the control actions in the form of discontinuous state functions like the on-and-off operation of the converters. SMC in the DC–DC converter has two forms, namely single loop SMC and Cascade SMC [25, 26].

The principal control parameter of the SMC is the sliding surface which is obtained from the system error signal in the open-loop condition. The involved variables provide a fast transient response along with the tracking of a specific reference signal path to achieve the desired dynamic response.

Some techniques have been investigated to improve the performance of the sliding mode control [27]. The addition of a PI voltage compensator in the outer loop being combined with the sliding mode current controller in the inner loop is proposed in [28]. It is compared to the use of a multi-predictive controller (MPC) on a boost converter. The combination of sliding mode control and the MPC was also explored in [29] with the purpose to control the output voltage of a boost converter. In [30], an SMC using PI switching surface for chaotic systems was developed with the presence of uncertainties and external disturbances. The unknown nonlinear functions were approached using fuzzy logic systems whereas the Lyapunov stability criterion was applied during the parameter adaptation design as well as stability evaluation.

There have been many research investigations on the use of SMC on the various topology of a DC–DC converter, but only a few are found concerning the Zeta converter [21, 31–33]. SMC is commonly used for systems having a non-linear response such as the Zeta converter. Zeta converter offers some advantages, especially that it can produce higher or lower output voltage than its respective input and that the output voltage is of the same polarity as the input [34]. However, in an open-loop configuration, it experiences a high transient overshoot and a long time duration before reaching the steady-state condition.

In this paper, the sliding mode control is used to adjust the Zeta converter output voltage, by considering the variation of the input voltage as well as the load condition. It is considered to accelerate the transient response, reduce the overshoot, and produce a constant voltage on the output side of the Zeta converter. The use of proportional-integral-differential (PID) control is chosen as comparison [35, 36].

In some previous studies, the PID controller on the Zeta converter was used to produce a good output response in the converter operating area. The voltage response on the Zeta converter with the PID controller is constant, even though there is a change in the input voltage as well as in the load. However, when there is a change in parameters such as input voltage, load size, and reference voltage outside the converter operating area, the system response becomes unstable and the PID controller cannot improve the response.

The use of PI-SMC to regulate the output voltage on the Zeta converter is presented in this research. The SMC is designed to provide the expected output voltage with a fast response and minimal errors. The results are compared with the performance of the PID controller on the Zeta converter. In the simulation tests, changes in input voltage, load, and reference voltage were evaluated.

The organization of this paper is made as follows. The next section is used to elaborate on the proposed method, consisting of the modeling of the Zeta converter and the description of the PI-SMC design. The following section presents the results of the study, containing the exploration of the output voltage response of the Zeta converter with a variation of the input voltage, the reference voltage, and the load condition, both using the considered PI-SMC method and the PID method as a comparison.

2. PROPOSED METHOD

The description of the PI-SMC method on the Zeta converter is started with the steps to model the Zeta converter and is followed by the elaboration of the PI-SMC method.

2.1. Zeta converter modeling

The Zeta converter considered in this paper uses two capacitors, two inductors, 1 diode, and 1 MOSFET, as seen in Fig. 1. L_1, L_2, C_1, C_2, R, V_s are subsequently the first inductor, the second inductor, the first capacitor, the second capacitor, the load resistor, and the input voltage. This converter is categorized as the DC–DC converter in general, which uses a switching technique to adjust the output voltage.
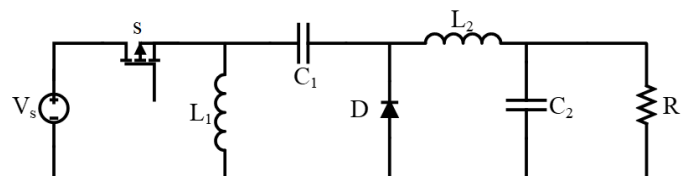

Fig. 1. Zeta converter circuit

In an ideal condition, the use of two capacitors and two inductors makes the Zeta converter classified as the fourth-order converter because it produces a 4th order equation [37]. The Zeta converter resembles a buck-boost converter, but with an output voltage of the same polarity as the input voltage.

The equivalent circuit of the Zeta converter circuit under the closed- and opened-switch conditions are shown in Fig. 2 and Fig. 3, respectively. The application of Kirchhoff voltage law
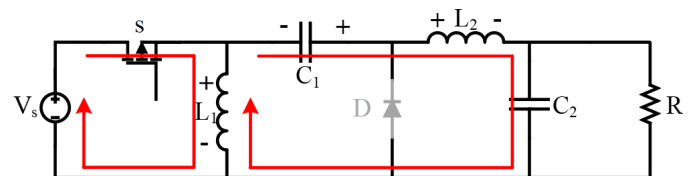

Fig. 2. Zeta converter circuit in closed-switch condition

2

Bull. Pol. Acad. Sci. Tech. Sci., vol. 70, no. 3, e140952, 2022

(KVL) and Kirchhoff current law (KCL) to the circuit shown in Figs. 2 and 3 is used to obtain the circuit equations of the Zeta converter under closed- and opened-switch conditions. When the switch is ON, as can be observed in Fig. 2, the input and output currents of the inductors increase linearly and the current in the diode is equal to zero.
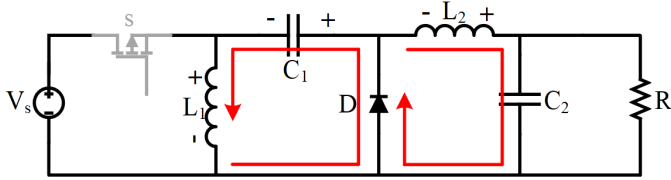

Fig. 3. Zeta converter circuit in opened-switch condition

By using Kirchhoff's Voltage Law on the circuit of closed-switch condition in Fig. 2, the sum of voltage along the left-side loop is stated in equation (1). By stating the voltage across the inductor L_1 using its proportionality to the multiplication of inductance and the change of current through the inductor, equations (2) and (3) are obtained

$$V_{L1} - V_s = 0, \tag{1}$$

$$L_1 \frac{\mathrm{d}i_{L1}}{\mathrm{d}t} = V_s, \tag{2}$$

$$\frac{\mathrm{d}i_{L1}}{\mathrm{d}t} = \frac{V_s}{L_1}. \tag{3}$$

Implementing Kirchhoff's Voltage Law on the right-side loop of Fig. 2 results in equation (4). Replacing the voltage across the inductor with its proportionality to the multiplication of inductance and the change of current through the inductor produces equations (5) and (6). The change of current through the inductor L_2 is stated in equation (6)

$$V_{L2} - V_{C1} + V_{C2} - V_S = 0, \tag{4}$$

$$L_2 \frac{\mathrm{d}i_{L2}}{\mathrm{d}t} = V_S + V_{C1} - V_{C2}, \tag{5}$$

$$\frac{\mathrm{d}i_{L2}}{\mathrm{d}t} = \frac{V_s}{L2} + \frac{V_{C1}}{L2} - \frac{V_{C2}}{L2}. \tag{6}$$

By using Kirchhoff's Current Law, the current through the capacitor C_1 is obtained using equation (7), while the change in voltage across the capacitor C_1 is obtained using equations (8) and (9), by replacing the current through the capacitor with its proportionality to the multiplication of capacitance and the change in voltage across the capacitor

$$i_{C1} + i_{L2} = 0, \tag{7}$$

$$C_1 \frac{\mathrm{d}V_{C1}}{\mathrm{d}t} = -i_{L2}, \tag{8}$$

$$\frac{\mathrm{d}V_{C1}}{\mathrm{d}t} = \frac{-i_{L2}}{C_1}. \tag{9}$$

The change in voltage across the capacitor C_2 is obtained using equations (10)–(12)

$$i_{C2} - i_{L2} + i_{RL} = 0, \tag{10}$$

$$C_2 \frac{\mathrm{d}V_{C2}}{\mathrm{d}t} = i_{L2} - i_{RL}, \tag{11}$$

$$\frac{\mathrm{d}V_{C2}}{\mathrm{d}t} = \frac{i_{L2}}{C_2} - \frac{V_{C2}}{R_L C_2}. \tag{12}$$

The differential equations in (3), (6), (9), and (12) can be presented in a form of a matrix to make the state-space equation of the Zeta converter under the ON-switch condition, as given in equation (13)

$$\begin{bmatrix} \frac{\mathrm{d}i_{L1}}{\mathrm{d}t} \\ \frac{\mathrm{d}i_{L2}}{\mathrm{d}t} \\ \frac{\mathrm{d}v_{C1}}{\mathrm{d}t} \\ \frac{\mathrm{d}v_{C2}}{\mathrm{d}t} \end{bmatrix} = \begin{bmatrix} 0 & 0 & 0 & 0 \\ 0 & 0 & \frac{1}{L_2} & -\frac{1}{L_2} \\ 0 & -\frac{1}{C_1} & 0 & 0 \\ 0 & \frac{1}{C_2} & 0 & -\frac{1}{R_L C_2} \end{bmatrix} \begin{bmatrix} i_{L1} \\ i_{L2} \\ v_{c1} \\ v_{c2} \end{bmatrix} + \begin{bmatrix} \frac{1}{L_1} \\ \frac{1}{L_2} \\ 0 \\ 0 \end{bmatrix} [V_s]. \tag{13}$$

Zeta converter circuit analysis when the switch is opened (in OFF condition) is based on Fig. 3. As can be observed, the diode will be forward-biased because the voltage at the anode is greater than the cathode so that the input and output currents of the inductors (i_{L1} and i_{L1}) will decrease linearly.

By using Kirchhoff's Voltage Law on the circuit of opened-switch condition, the sum of voltage along the left-side loop of Fig. 3 is stated in equation (14). By stating the voltage across the inductor L_1 using its proportionality to the multiplication of inductance and the change of current through the inductor, equations (15) and (16) are obtained. The change of current through the inductor L_1 under the OFF-switch condition is stated in equation (16)

$$V_{L1} + V_{C1} = 0, \tag{14}$$

$$L_1 \frac{\mathrm{d}i_{L1}}{\mathrm{d}t} = -V_{C1}, \tag{15}$$

$$\frac{\mathrm{d}i_{L1}}{\mathrm{d}t} = -\frac{V_{C1}}{L_1}. \tag{16}$$

Implementing Kirchhoff's Voltage Law on the right-side loop of Fig. 3, and then replacing the voltage across the inductor L_2 with its proportionality to the multiplication of inductance and the change of current through the inductor produces equation (17). The change of current through the inductor L_2 under OFF-switch condition is stated in equation (18)

$$L_2 \frac{\mathrm{d}i_{L2}}{\mathrm{d}t} = -V_{C2}, \tag{17}$$

$$\frac{\mathrm{d}i_{L2}}{\mathrm{d}t} = -\frac{V_{C2}}{L_2}. \tag{18}$$

By using Kirchhoff's Current Law, the current through the capacitor C_1 under OFF-switch condition is obtained using equa-

tion (19), while the change in voltage across the capacitor C_1 is obtained using equations (20) and (21), by replacing the current through the capacitor with its proportionality to the multiplication of capacitance and the change in voltage across the capacitor

$$i_{C1} + i_{L1} = 0, \tag{19}$$

$$C_1 \frac{\mathrm{d}V_{C1}}{\mathrm{d}t} + i_{L1} = 0, \tag{20}$$

$$\frac{\mathrm{d}V_{C1}}{\mathrm{d}t} = -\frac{i_{L1}}{C_1}. \tag{21}$$

The change in voltage across the capacitor C_2 under the OFF-switch condition is obtained using equations (22)–(24)

$$i_{C2} - i_{L2} + i_{RL} = 0, \tag{22}$$

$$C_2 \frac{\mathrm{d}V_{C2}}{\mathrm{d}t} - i_{L2} + i_{RL} = 0, \tag{23}$$

$$\frac{\mathrm{d}V_{C2}}{\mathrm{d}t} = \frac{i_{L2}}{C_2} - \frac{V_{C2}}{R_L C_2}. \tag{24}$$

The differential equations in (16), (18), (21), and (24) can be presented in a form of a matrix to make the state-space equation of the Zeta converter under the OFF-switch condition, as given in equation (25)

$$\begin{bmatrix} \dfrac{\mathrm{d}i_{L1}}{\mathrm{d}t} \\ \dfrac{\mathrm{d}i_{L2}}{\mathrm{d}t} \\ \dfrac{\mathrm{d}v_{C1}}{\mathrm{d}t} \\ \dfrac{\mathrm{d}v_{C2}}{\mathrm{d}t} \end{bmatrix} = \begin{bmatrix} 0 & 0 & -\dfrac{1}{L_1} & 0 \\ 0 & 0 & 0 & -\dfrac{1}{L_2} \\ -\dfrac{1}{C_1} & 0 & 0 & 0 \\ 0 & \dfrac{1}{C_2} & 0 & -\dfrac{1}{R_L C_2} \end{bmatrix} \begin{bmatrix} i_{L1} \\ i_{L2} \\ v_{c1} \\ v_{c2} \end{bmatrix} + \begin{bmatrix} 0 \\ 0 \\ 0 \\ 0 \end{bmatrix} [V_s]. \tag{25}$$

State-space averaging is furthermore explored to approximate the switching converter as a continuous linear system [38–41].

2.2. Design of PI-sliding mode control

There are two duty-cycle values in sliding mode control, which are the equivalent control signal (U_{eq}) and natural control signal (U_N) as shown in equation (26)

$$U = U_{\mathrm{eq}} + U_N. \tag{26}$$

At steady-state conditions, the reference current x_1^* is determined using the reference voltage according to equation (27)

$$x_1^* = \frac{V_{\mathrm{ref}}^2}{RV_s}. \tag{27}$$

Determining the sliding surface (S) on the Zeta converter is carried out by using an error function (e), where the reference used is the current in inductor $L_1(x_1)$. It is to remember that x_1 represents i_{L1}, x_2 represents i_{L2}, x_3 represents v_{C1}, and x_4 represents v_{C2}. After the inductor reference current (x_1^*) is determined,

the next step is to substitute (x_1^*) into equation (28) to obtain equation (29)

$$S = ke + \lambda \int e\,\mathrm{d}t, \tag{28}$$

where λ is a constant sliding surface parameter. The symbol e represents the difference between the current in inductor L_1 in real time and the reference current in inductor L_1. The sliding surface equation is obtained by setting $\lambda = 1$ as follows

$$S = k(x_1 - x_1^*) + \int (x_1 - x_1^*)\,\mathrm{d}t. \tag{29}$$

The next step is to find the U_{eq} value by lowering the sliding surface equation to zero, as given in equations (30) and (31)

$$0 = \dot{S} = \frac{\mathrm{d}}{\mathrm{d}t}(kx_1 + e), \tag{30}$$

$$U_{\mathrm{eq}} = \frac{kx_3 - L_1 e}{k(x_3 + V_s)}. \tag{31}$$

After U_{eq} is obtained, the next step is to determine the U_N. The U_N value is determined based on the Lyapunov stability theory [17], as in equation (32)

$$V = S\dot{S}. \tag{32}$$

The expected conditions should satisfy the requirement in equation (33)

$$\dot{S} < 0. \tag{33}$$

The first step is to determine the derivative of the sliding surface ($\dot{S}$), so that the expected error is close to zero. Equation (34) is the derivative of the S formula in (29)

$$\dot{S} = k\dot{x}_1 + e. \tag{34}$$

Substituting further the equation $\dot{x}_1$ into $\dot{S}$ results in equation (35)

$$\dot{S} = \left(\frac{-kx_3 + kx_3 U + kV_s U + L_1 e}{L_1} \right). \tag{35}$$

By replacing U with (26), the $\dot{S}$ equation is obtained in equation (36)

$$\dot{S} = \left(\frac{-kx_3 + kx_3 (U_{\mathrm{eq}} + U_N) + kV_s (U_{\mathrm{eq}} + U_N) + L_1 e}{L_1} \right). \tag{36}$$

Substituting U_{eq} in equation (31) into equation (36) to result in equation (37) and simplifying further to produce equation (38) to conform the required condition given by equation (33) would result in equation (39)

$$\dot{S} = \left(\frac{-kx_3 + (kx_3 + kV_s)\left(\dfrac{kx_3 - L_1 e}{k(x_3 + V_s)} + U_N \right) + L_1 e}{L_1} \right), \tag{37}$$

4

Bull. Pol. Acad. Sci. Tech. Sci., vol. 70, no. 3, p. e140952, 2022

$$\dot{S} = \left(\frac{U_N k (x_3 + V_s)}{L_1} \right), \qquad (38)$$

$$\left(\frac{U_N k (x_3 + V_s)}{L_1} \right) < 0. \qquad (39)$$

To fulfill the Lyapunov stability criterion, the U_N scores are determined as equation (40)

$$U_N = \frac{L_1}{k (x_3 + V_s)} \text{sign}(S). \qquad (40)$$

The required duty-cycle value is obtained through the addition of U_{eq} and U_N. The derivation of the duty-cycle equation at the SMC is given by substitution into equation (26) to obtain equation (41)

$$U = \frac{kx_3 - L_1 e}{k (x_3 + V_s)} + \left(\frac{L_1}{k (x_3 + V_s)} \text{sign}(S) \right). \qquad (41)$$

U is the duty cycle of the output from the SMC which will regulate the switching of the MOSFET electronic switch components on the Zeta converter.

3. RESULTS AND ANALYSIS
The results of the study were obtained based on the proposed system scheme given in Fig. 4.
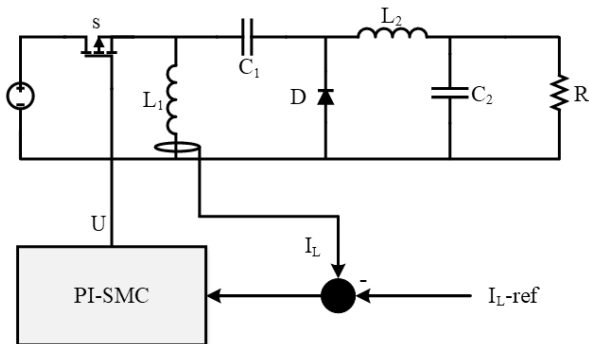
Fig. 4. Proposed system

The system was exposed to some disturbances in the form of changes in input voltage, reference voltage, and load. The simulation was carried out over a certain time duration and the disturbance was given at the time of 0.01 sec. The first test was performed by changing the input voltage while maintaining constant the reference voltage and load. The second test was done by changing the reference voltage while keeping the input voltage and load constant. The third test was carried out by changing the load condition while maintaining the fixed input voltage and reference voltage. The specification of the considered components in this study is presented in Table 1.

3.1. The influence of the change in input voltage
The change in input voltage was achieved by using 5 different values: 6 V, 12 V, 18 V, 30 V, and 36 V. The simulation results are indicated in Table 2. A comparison of the recovery time (t_{rec})

Table 1
Converter specification

No	Symbol	Value	Parameter
1	V_s	24 V	Input Voltage
2	V_o	12 V	Output Voltage
3	f	20000 Hz	Switching Frequency
4	R	100 Ω	Load Resistor
5	L_1	100 µH	Inductor 1
6	L_2	50 mH	Inductor 2
7	C_1	47 µF	Capacitor 1
8	C_2	6.8 µF	Capacitor 2

Table 2
Control response of the proposed method when the input voltage is changing

V_{in} (V)	V_{ref} (V)	R (Ω)	SMC		PID	
			t_{rec} (s)	$\|\Delta V\|$ (V)	t_{rec} (s)	$\|\Delta V\|$ (V)
6			0.0605	0.56	–	–
12			0.02178	0.49	–	–
18	12	100	0.01471	0.21	–	–
30			0.01012	0.15	0.01979	3.08
36			0.02008	0.28	0.03282	5.96

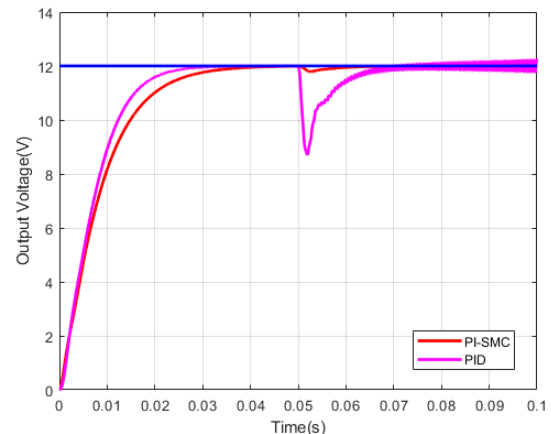curves obtained using the SMC and PID controllers is shown in Fig. 5.

Fig. 5. Output voltage response when the input voltage is changed to 6 V

As can be observed in Table 2, in PID controllers when the input voltage changes to below than initial value, the PID controller is not able to continue simulation because of unstable conditions. Figure 5 depicts the comparison graph of the response for SMC and PID controllers when the input voltage changes from 24 V to 6 V. It is shown that the system with SMC reaches the steady state slower than the PID controller in the beginning. When the input voltage changes the PID controller has a high overshoot of –3.17 V when compared to SMC that

Bull. Pol. Acad. Sci. Tech. Sci., vol. 70, no. 3, p. e140952, 2022

5

has an overshoot of less than 0.6 V. The proposed controller requires 0.060 s to reach the reference voltage, while at the same time the PID controller keeps away the steady state.

The severity of the occurring overshoot depends on the difference between the input voltage during normal conditions and during disturbances. If during the disturbance the input voltage is below the input voltage during normal conditions, there will be a negative overshoot. The greater the difference in input voltage between normal conditions and during interference, the greater the overshoot.

The smallest delta error or voltage deviation (ΔV) occurs when the input voltage becomes 30 V and the largest delta error occurs when the input voltage becomes 6 V. Based on these results, it is shown that a smaller input voltage generates a higher voltage deviation (ΔV). However, the voltage deviation (ΔV) becomes higher when the input voltage changes to 36 V.

3.2. The influence of the change in reference voltage

The change in reference voltage was achieved by using 5 different values: 6 V, 9 V, 15 V, 18 V, and 21 V, as given in Table 3. Figure 6 shows a graph of the output response of the SMC and PID controllers on changing reference voltage to 21 V.

Table 3

Control response of the proposed method when the reference voltage is changing

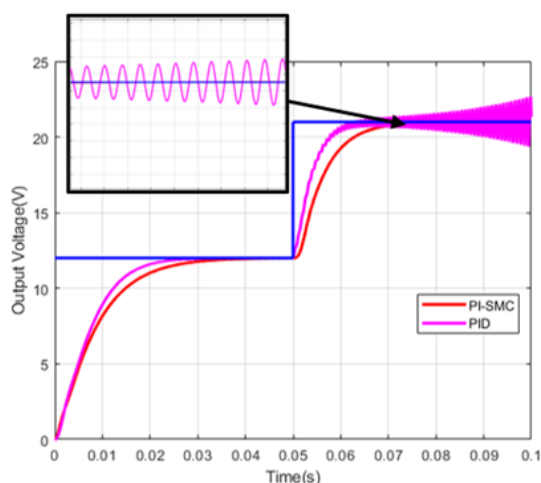| V_{in} (V)	V_{ref} (V)	R (Ω)	SMC		PID	
			t_{rec} (s)	$|\Delta V|$ (V)	t_{rec} (s)	$|\Delta V|$ (V)
24	6	100	0.0434	0	0.0815	29.07
	9		0.0407	0	–	–
	15		0.0374	0	–	–
	18		0.0369	0	–	–
	21		0.0362	0	–	–

Fig. 6. Output voltage response when the reference voltage is changed to 21 V

When the reference voltage changes to a greater value than the reference voltage, the SMC results in a recovery time value

of less than 0.045 s. Based on these results, it can be concluded that for the greater reference voltage, the recovery time is quite fast for the proposed controller. Meanwhile, the smaller the reference voltage, the longer the recovery time. The PID controller produces an oscillation when the reference voltage changes, and it is not possible to continue the simulation

3.3. The influence of the change in load resistor

In the last scenario, the loads used are 50 Ω, 75 Ω, 125 Ω, 150 Ω, and 175 Ω. The performances of each controller are presented in Table 4. The small delta error or voltage deviation occurs when the load becomes 125 Ω, which is 1.31 V for the proposed controller and 1.2 V for the PID controller. The proposed control results in faster recovery times than the PID controller, as shown in Fig. 7. It can be seen obviously that the proposed controller is able to reach the voltage reference more rapidly than the other method. In the PID method, the response has low settling time and small oscillation during steady state.

Table 4

Control response of the proposed method when the load resistor is changing

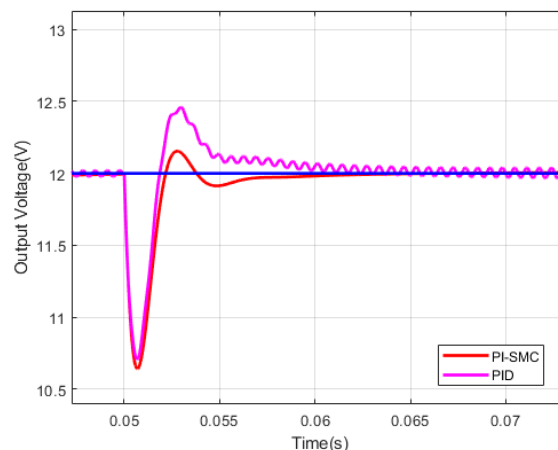| V^{in} (V)	V_{ref} (V)	R (Ω)	SMC		PID	
			t_{rec} (s)	$|\Delta V|$ (V)	t_{rec} (s)	$|\Delta V|$ (V)
24	12	50	0.0088	4.175	0.01987	3.981
		75	0.00814	1.75	0.01695	1.67
		125	0.00957	1.31	0.01617	1.2
		150	0.01308	2.33	0.02134	2.14
		175	0.02977	3.14	0.0336	2.89

Fig. 7. Output voltage response when the load resistor is changed to 75 Ω

4. CONCLUSIONS

Based on the results of simulation and analysis in this study, the following conclusions can be drawn. The PI-SMC method is determined by sliding surface reference, which can be voltage, current, and power. Furthermore, the sliding surface equation is determined to get the duty cycle for the switching on the

6

Bull. Pol. Acad. Sci. Tech. Sci., vol. 70, no. 3, p. e140952, 2022

MOSFET. The use of PI-SMC produces a faster time to reach the steady-state condition of the Zeta converter output voltage response, being compared to the use of a PID controller. When there is a change in input voltage, reference voltage, and load, the use of PI-SMC can reach the steady-state conditions faster than the use of PID control. In addition, the Zeta converter using SMC has a faster recovery time during disturbances than that using the PID controller.

ACKNOWLEDGEMENTS

REFERENCES

[1] REN21, "Distributed Renewables for Energy Access," in *Renewables 2021 Global Status Report*, Paris: REN21 Secretariat, 2021. [Online]. Available: https://www.ren21.net/gsr-2021/chapters/chapter_04/chapter_04/ [Accessed: 08. Nov. 2021]

[2] A. Mehravaran, A. Derhem, and M. Nassereddine, "Building-Integrated Photovoltaics (BIPV) for Residential and Industrial Properties," in *Proc. Advances in Science and Engineering Technology International Conferences (ASET)*, 2019, pp. 1–6, doi: 10.1109/ICASET.2019.8714466.

[3] C.W.X. Ng, J. Zhang, and S.E.R. Tay, "A Tropical Case Study Quantifying Solar Irradiance Collected on a Car Roof for Vehicle Integrated Photovoltaics Towards Low-Carbon Cities," in *Proc. 47th IEEE Photovoltaic Specialists Conference (PVSC)*, 2020, pp. 2461–2464, doi: 10.1109/PVSC45281.2020.9300351.

[4] J. Dawidziuk, "Review and comparison of high efficiency high power boost DC/DC converters for photovoltaic applications," *Bull. Pol. Acad. Sci. Tech. Sci.*, vol. 59, no. 4, pp. 499–506, 2011, doi: 10.2478/v10175-011-0061-7.

[5] S. Moury and J. Lam, "An Integrated PV-Battery Soft-switched Power Converter with MPPT and Voltage Regulation," in *Proc. IEEE Energy Conversion Congress and Exposition (ECCE)*, 2019, pp. 3433–3440, doi: 10.1109/ECCE.2019.8913273.

[6] S. Moury and J. Lam, "A Soft-Switched Power Module With Integrated Battery Interface for Photovoltaic-Battery Power Architecture," *IEEE J. Emerging Sel. Top. Power Electron.*, vol. 8, no. 3, pp. 3090–3110, 2020, doi: 10.1109/JESTPE.2019.2916733.

[7] R.K. Subroto, L. Ardhenta and E. Maulana, "A novel of adaptive sliding mode controller with observer for DC/DC boost converters in photovoltaic system," in *Proc. 5th International Conference on Electrical, Electronics and Information Engineering (ICEEIE)*, 2017, pp. 9–14, doi: 10.1109/ICEEIE.2017.8328754.

[8] R.K. Subroto, L. Ardhenta and K. Lian, "Observer Based Adaptive PI Sliding Mode Controller for Cuk Converter," in *Proc. 6th International Conference on Instrumentation, Control, and Automation (ICA)*, 2019, pp. 82–87, doi: 10.1109/ICA.2019.8916718.

[9] L. Ardhenta, P. Kuswiradyo, and R.K. Subroto, "Model direct adaptive control of buck converter by using MRAC," *Int. J. Innov.*

[10] L. Ardhenta and R.K. Subroto, "Application of direct MRAC in PI controller for DC–DC boost converter," *Int. J. Power Electron. Drive Syst.*, pp. 851–858, 2020, doi: 10.11591/ijpeds.v11.i2.pp851-858.

[11] A. Kawa and R. Stala, "The flying-capacitor SEPIC converter with the balancing circuit," *Arch. Electr. Eng.*, vol. 65, no. 3, pp. 411–424, 2016, doi: 10.2478/v10175-011-0061-7.

[12] F. Bayat, M. Karimi, and A. Taheri, "Robust output regulation of Zeta converter with load/input variations: LMI approach," *Control Eng. Pract.*, vol. 84, pp. 102–111, 2019, doi: 10.1016/j.conengprac.2018.10.023.

[13] P.R. Babu, S.R. Prasath, and R. Kiruthika, "Simulation and performance analysis of CCM Zeta converter with PID controller," in *Proc. International Conference on Circuits, Power and Computing Technologies [ICCPCT-2015]*, 2015, pp. 1–7, doi: 10.1109/ICCPCT.2015.7159506.

[14] S. Arvind, R. Akshay and A. Sreedevi, "A novel constant frequency sliding mode control of DC–DC converters," in *Proc. IEEE 7th Power India International Conference (PIICON)*, 2016, pp. 1–6, doi: 10.1109/POWERI.2016.8077387.

[15] D.W. Hart. *Power Electronics*. New York: McGraw-Hill, 2011.

[16] K. Woranetsuttikul, K. Pinsuntia, N. Jumpasri, T. Nilsakorn, and W. Khanngern, "Comparison on performance between synchronous single-ended primary-inductor converter (SEPIC) and synchronous ZETA converter," in *Proc. International Electrical Engineering Congress (iEECON)*, 2014, pp. 1–4, doi: 10.1109/iEECON.2014.6925855.

[17] V.I. Utkin, "Sliding Mode Control: Mathematical Tools, Design and Applications," in *Nonlinear and Optimal Control Theory. Lecture Notes in Mathematics*, vol. 1932, Nistri P., Stefani G. (eds). Springer, Berlin, Heidelberg: Springer, 2008, doi: 10.1007/978-3-540-77653-6_5.

[18] L. Zarour, K. Abed, M. Hacil, and A. Borni, "Control and optimisation of photovoltaic water pumping system using sliding mode," *Bull. Pol. Acad. Sci. Tech. Sci.*, vol. 67, no. 3, pp. 605–611, 2019, doi: 10.24425/bpasts.2019.129658.

[19] D.K. Dash, P.K. Sadhu, and B. Subudhi, "Spider monkey optimization (SMO) – lattice Levenberg–Marquardt recursive least squares based grid synchronization control scheme for a three-phase PV system," *Arch. Control Sci.*, vol. 31, no. LXVII, pp. 707–730, 2021, doi: 10.24425/acs.2021.138698.

[20] K. Ogata. *Modern Control Engineering*. New Jersey: Prentice Hall, 2010, pp. 11–15, 18–21.

[21] S.K. Pandey, S.L. Patil, S.B. Phadke, and A.S. Deshpande, "Investigation of sliding mode control of higher order DC–DC converters," in *Proc. 7th India International Conference on Power Electronics (IICPE)*, 2016, pp. 1–5, doi: 10.1109/IICPE.2016.8079439.

[22] B.B. Naik and A.J. Mehta, "Sliding mode controller with modified sliding function for DC–DC Buck Converter," *ISA Trans.*, vol. 70, pp. 279–287, 2017, doi: 10.1016/j.isatra.2017.05.009.

[23] C.S. Sachin and S.G. Nayak, "Design and simulation for sliding mode control in DC–DC boost converter," in *Proc. 2nd International Conference on Communication and Electronics Systems (ICCES)*, 2017, pp. 440–445, doi: 10.1109/CESYS.2017.8321317.

[24] J. Cao, Q. Chen, L. Zhang, and S. Quan, "Sliding mode control of bidirectional DC/DC converter," in *Proc. 33rd Youth Academic Annual Conference of Chinese Association of Automation (YAC)*, 2018, pp. 717–721, doi: 10.1109/YAC.2018.8406465.

Rini Nur Hasanah *et al.*

[25] Rashmi, J. Manohar, and K.S. Rajesh, "A comparative study and performance analysis of synchronous SEPIC Converter and synchronous Zeta Converter by using PV system with MPPT technique," in *Proc. IEEE 1st International Conference on Power Electronics, Intelligent Control and Energy Systems (ICPEICES)*, 2016, pp. 1–6, doi: 10.1109/ICPEICES.2016.7853212.

[26] K.O. Vijay and P. Sriramalakshmi, " Comparison between Zeta Converter and Boost Converter using Sliding Mode Controller," *Int. J. Res. Tech. (IJERT)*, vol. 5, no. 7, pp. 368–373, 2016, doi: 10.17577/IJERTV5IS070322.

[27] H.M. Solaiman, M.M. Hasan, A. Mohammad, S.R. Kawsar, and M.A. Hassan, "Performance analysis of DC to DC boost converter using different control methods," in *Proc. IEEE International Conference on Electrical, Computer and Communication Technologies (ICECCT)*, 2015, pp. 1–5, doi: 10.1109/ICECCT.2015.7226007.

[28] D. Plaza, R. De Keyser and J. Bonilla, "Model Predictive and sliding mode control of a Boost converter," in *Proc. International Symposium on Power Electronics, Electrical Drives, Automation and Motion*, 2008, pp. 37-42, doi: 10.1109/SPEEDHAM.2008.4581242.

[29] B. Talbi, F. Krim, A. Laib, A. Sahli, and A. Krama, "PI-MPC Switching Control for DC–DC Boost Converter using an Adaptive Sliding Mode Observer," in *Proc. International Conference on Electrical Engineering (ICEE)*, 2020, pp. 1–5, doi: 10.1109/ICEE49691.2020.9249934.

[30] D. Cui, H. Zhu, and H. Liu, "Adaptive fuzzy control for a class of uncertain chaotic systems based on proportional-integral sliding mode control approach," in *Proc. Chinese Control and Decision Conference (CCDC)*, 2018, pp. 589–593, doi: 10.1109/CCDC.2018.8407200.

[31] M.S. Diab, A. Elserougi, A.S. Abdel-khalik, A.M. Massoud and S. Ahmed, "A Zeta-converter based four-switch three-phase DC-AC inverter," in *Proc. IEEE Energy Conversion Congress and Exposition (ECCE)*, 2015, pp. 4671–4677, doi: 10.1109/ECCE.2015.7310320.

[32] M. Ebadpour and F. Radmand, "Hyper-Plane Sliding Mode Control of Non-Minimum Phase Grid-Connected Zeta Converter," in *Proc. 12th Power Electronics, Drive Systems, and Technologies Conference (PEDSTC)*, 2021, pp. 1–5, doi: 10.1109/PEDSTC52094.2021.9405835.

[33] C.-Y. Chan, "Adaptive Sliding-Mode Control of a Novel Buck-Boost Converter Based on Zeta Converter," *IEEE Trans. Circuits Syst. II Express Briefs*, vol. 69, no. 3, pp. 1307–1311, 2022, doi: 10.1109/TCSII.2021.3107315.

[34] K. Durgadevi and R. Karthik, "Performance Analysis of Zeta Converter Using Classical PID and Fractional Order PID Controller," in *Proc. International Conference on Power, Energy, Control and Transmission Systems (ICPECTS)*, 2018, pp. 312–317, doi: 10.1109/ICPECTS.2018.8521573.

[35] S. Tan, Y.M. Lai, and C.K. Tse, "General Design Issues of Sliding-Mode Controllers in DC–DC Converters," *IEEE Trans. Ind. Electron.* vol. 55, no. 3, pp. 1160–1174, 2008, doi: 10.1109/TIE.2007.909058.

[36] B. Saleh, A. Teirelbar, and A. Wasfi, "A DC/DC buck-boost converter control using sliding surface mode controller and adaptive PID controller," in *Proc. 22nd European Conference on Power Electronics and Applications (EPE'20 ECCE Europe)*, 2020, pp. P.1–P.8, doi: 10.23919/EPE20ECCEEurope43536.2020.9215853.

[37] S. Misal and M. Veerachary, "Analysis of a Fourth-Order Step-Down Converter," *IEEE Trans. Ind. Appl.*, vol. 56, no. 3, pp. 2773–2787, 2020, doi: 10.1109/TIA.2020.2975500.

[38] J. Mahdavi, A. Emaadi, M.D. Bellar, and M. Ehsani, "Analysis of power electronic converters using the generalized state-space averaging approach," *IEEE Trans. Circuits Syst. I: Fundam. Theory Appl.*, vol. 44, no. 8, pp. 767–770, 1997, doi: 10.1109/81.611275.

[39] D. Yan, C. Yang, L. Hang, Y. He, P. Luo, L. Shen and P. Zeng, "Review of general modeling approaches of power converters," *Chin. J. Electr. Eng.*, vol. 7, no. 1, pp. 27–36, 2021, doi: 10.23919/CJEE.2021.000002.

[40] A. Ravi, S.L. Phen, P.A. Pandi, J.J. Gnanachandran, N. Subramanian, and N.S. Pratheepa, "The State Space Average Model of Cuk Converter Fed From Photo Voltaic Array," in *Proc. 5th International Conference on Trends in Electronics and Informatics (ICOEI)*, 2021, pp. 349–355, doi: 10.1109/ICOEI51242.2021.9453017.

[41] R.H.G. Tan and L.Y.H. Hoo, "DC–DC converter modeling and simulation using state space approach," in *Proc. IEEE Conference on Energy Conversion (CENCON)*, 2015, pp. 42–47, doi: 10.1109/CENCON.2015.7409511.

8

Bull. Pol. Acad. Sci. Tech. Sci., vol. 70, no. 3, p. e140952, 2022